Supplementary Information

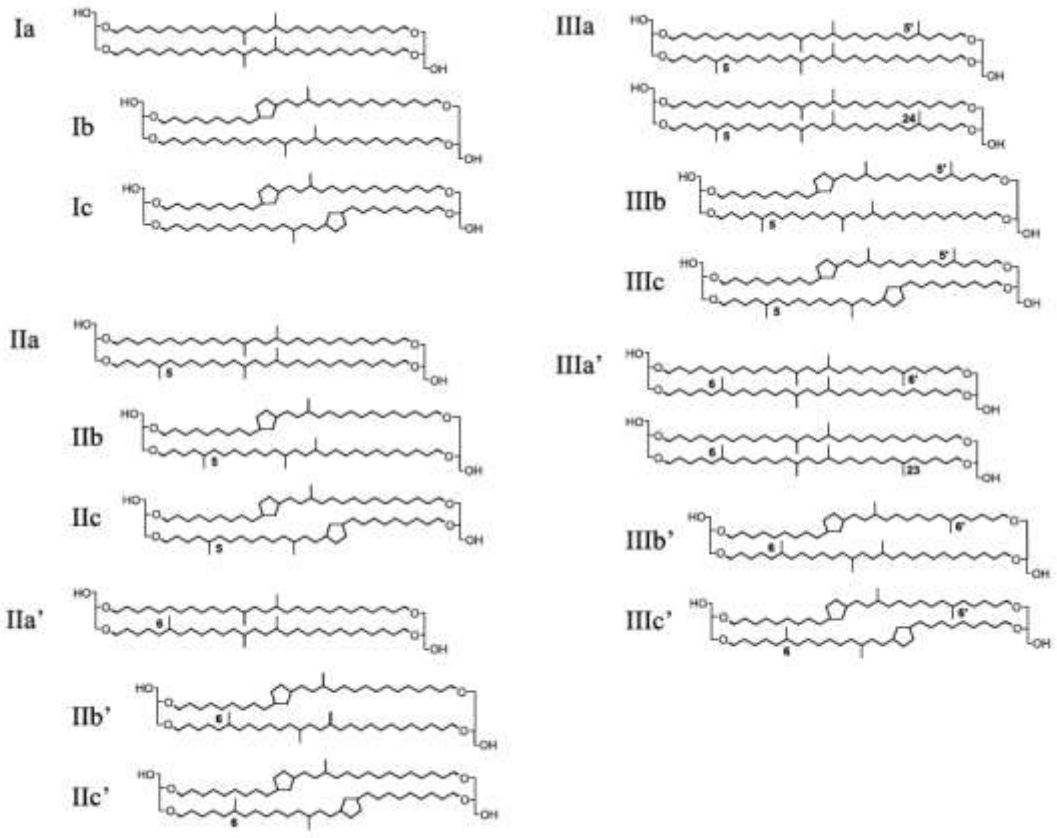

Figure S1. Molecular structures of all 15 brGDGTs (I-III). The molecules designated with a prime symbol are referred to as the 6-methyl brGDGTs.

(a) **(b)**

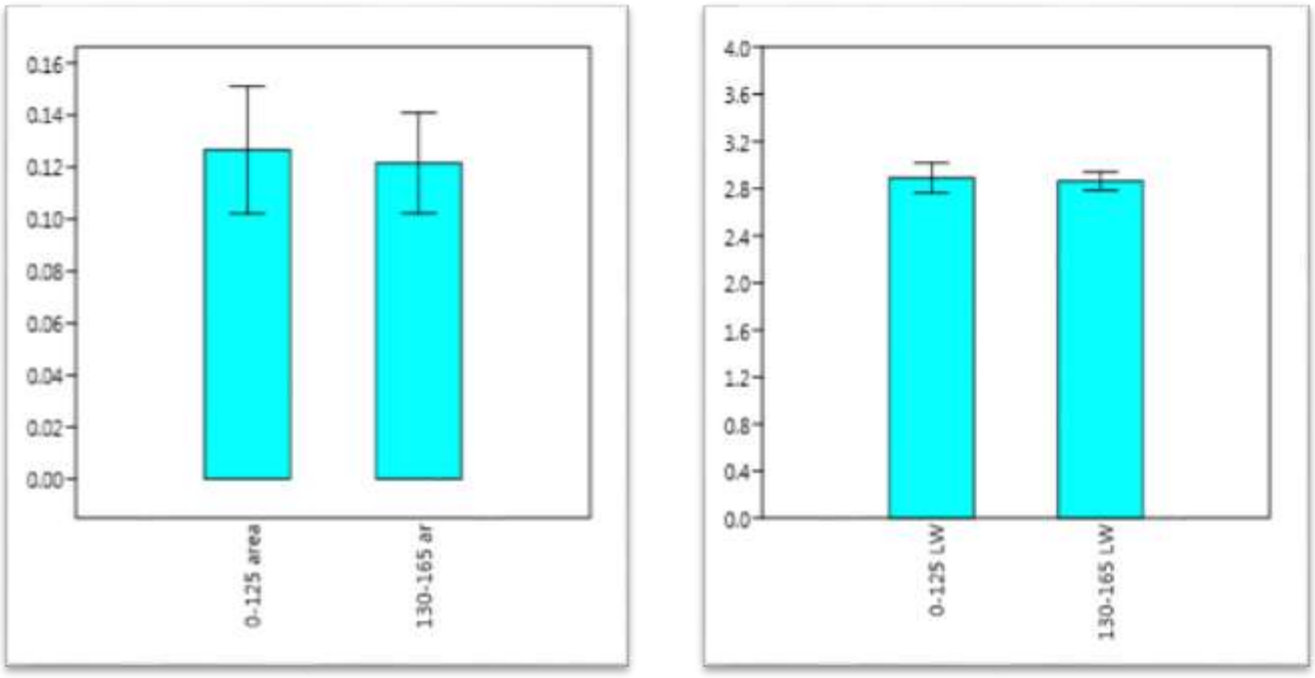

Figure S2. A comparison of the area (a, mm^2) and shape (b, length to width) of the uppermost samples (130–165) that have a higher mean charcoal concentration, and the lowermost samples (0–125).

depthID	18050
pdfmaxage	3.62E+06
sigma1plus	1.50E+06
sigma1minus	4.78E+05
sigma2plus	4.77E+06
sigma2minus	1.03E+06
burial_sim	[1×2000
pdf	[1×2000
exposure_meanvalue	11.8187
burial_meanvalue	3.5818
fval	0.0103

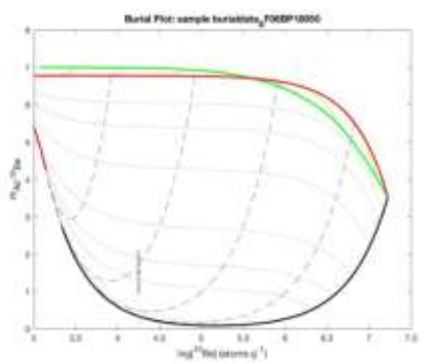

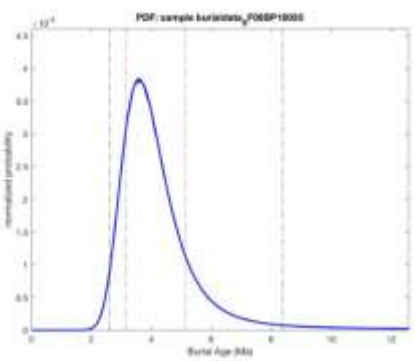

depthID	18097
pdfmaxage	3.94E+06
sigma1plus	3.66E+06
sigma1minus	4.77E+05
sigma2plus	8.69E+06
sigma2minus	1.22E+06
burial_sim	[1×2000
pdf	[1×2000

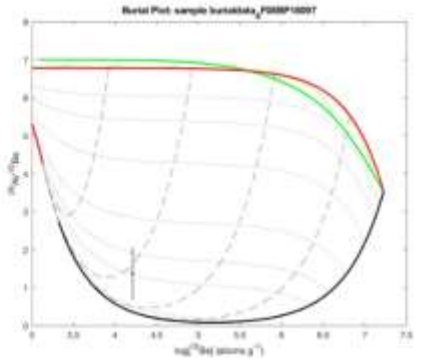

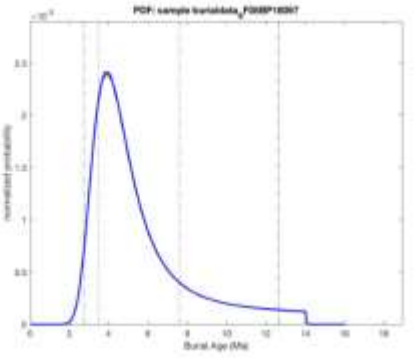

depthID	18155
pdfmaxage	4.07E+06
sigma1plus	5.79E+06
sigma1minus	3.51E+05
sigma2plus	9.11E+06
sigma2minus	1.31E+06
burial_sim	[1×2000
pdf	[1×2000

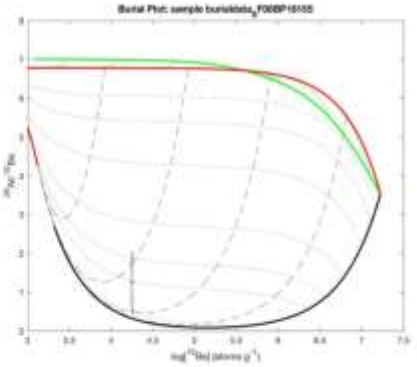

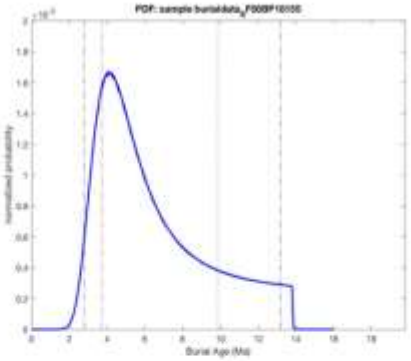

depthID	18222
pdfmaxage	3.95E+06
sigma1plus	1.49E+06
sigma1minus	4.31E+05
sigma2plus	4.43E+06
sigma2minus	9.74E+05
burial_sim	[1×2000
pdf	[1×2000
exposure_meanvalue	16.6957
burial_meanvalue	3.9513
fval	0.0147

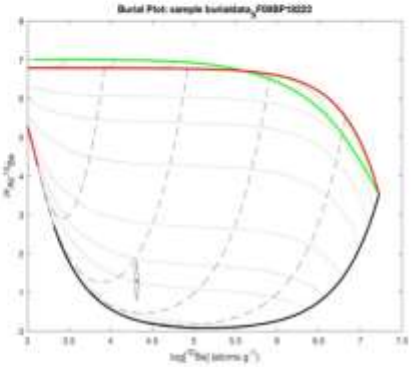

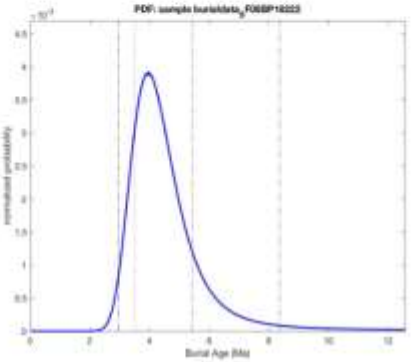

Figure S3. Burial age results. depthID: average initial sample depth, pdfmaxage: the most probable age as determined from the probability density function, sigma1plus and sigma1minus: the +/-1sigma errors in pdfmaxage, sigma2plus and sigma2minus: the +/- 2sigma errors in pdfmaxage, exposure_meanvalue: mean value of pre-buildup exposure age taken from FMINLBFGS optimization algorithm, burial_meanvalue: mean value of burial age taken from FMINLBFGS optimization algorithm. The 26Al/10Be vs. log10 10Be plots are unique for each mass depth. The generally horizontal dotted curves are burial isochrons, from top to bottom 0.25, 0.50, 1.0, 2.0, 3.0, 4.0. and 8.0 Ma, and the near-vertical dashed lines are pre-burial minimum exposure duration isochrons, from left to right 103, 104, 105, and 106 years. The PDF plots are probability distributions of 2000 solutions of the data.

Table S1. Fractional abundances of the brGDGTs found in the Beaver Pond sediments.

Sample Name	Ia	Ib	Ic	IIa	IIb	IIc	IIIa	IIIb	IIIc	IIa′	IIb′	IIc′	IIIa′	IIIb′	IIIc′
BP-A-02	0.08	0.05	0.01	0.15	0.05	0.00	0.27	0.01	0.00	0.12	0.05	0.00	0.21	0.01	0.00
BP-A-03	0.07	0.03	0.00	0.11	0.03	0.00	0.26	0.00	0.00	0.15	0.05	0.00	0.30	0.01	0.00
BP-A-04	0.12	0.04	0.00	0.13	0.03	0.00	0.23	0.00	0.00	0.15	0.04	0.00	0.25	0.01	0.00
06BP01	0.10	0.04	0.01	0.13	0.03	0.00	0.31	0.00	0.00	0.12	0.03	0.00	0.22	0.00	0.00
06BP16	0.11	0.04	0.00	0.15	0.03	0.00	0.30	0.00	0.00	0.13	0.03	0.00	0.20	0.00	0.00
06BP18*	0.11	0.03	0.00	0.15	0.02	0.00	0.29	0.00	0.00	0.14	0.03	0.00	0.21	0.00	0.00
06BP18*	0.11	0.03	0.00	0.15	0.02	0.00	0.29	0.00	0.00	0.13	0.03	0.00	0.21	0.00	0.00
BP-F-73*	0.10	0.04	0.00	0.19	0.03	0.00	0.26	0.00	0.00	0.14	0.03	0.00	0.19	0.01	0.00
BP-F-73*	0.11	0.05	0.00	0.22	0.04	0.00	0.21	0.00	0.00	0.16	0.04	0.00	0.15	0.01	0.00
BP-A-06	0.11	0.04	0.01	0.15	0.03	0.00	0.24	0.00	0.00	0.15	0.04	0.00	0.22	0.01	0.00
BP-A-07	0.13	0.04	0.01	0.16	0.03	0.00	0.23	0.00	0.00	0.15	0.04	0.00	0.20	0.01	0.00
06BP03	0.11	0.04	0.00	0.15	0.03	0.00	0.28	0.00	0.00	0.13	0.03	0.00	0.22	0.01	0.00
06BP05*	0.10	0.04	0.00	0.15	0.03	0.00	0.29	0.00	0.00	0.12	0.03	0.00	0.23	0.01	0.00
06BP05*	0.11	0.04	0.01	0.16	0.03	0.00	0.28	0.00	0.00	0.13	0.03	0.00	0.19	0.00	0.00
06BP07	0.13	0.04	0.00	0.19	0.03	0.00	0.28	0.00	0.00	0.13	0.03	0.00	0.16	0.00	0.00
06BP09	0.09	0.03	0.00	0.14	0.03	0.00	0.30	0.00	0.00	0.13	0.03	0.00	0.23	0.01	0.00
06BP11*	0.11	0.04	0.01	0.16	0.03	0.00	0.31	0.00	0.00	0.12	0.03	0.00	0.19	0.00	0.00
06BP11*	0.10	0.04	0.00	0.15	0.03	0.00	0.29	0.00	0.00	0.14	0.03	0.00	0.21	0.00	0.00
06BP13	0.11	0.04	0.00	0.15	0.03	0.00	0.30	0.00	0.00	0.13	0.03	0.00	0.20	0.00	0.00
06BP14*	0.10	0.04	0.00	0.15	0.03	0.00	0.29	0.00	0.00	0.13	0.03	0.00	0.21	0.00	0.00
06BP14*	0.10	0.04	0.00	0.14	0.03	0.00	0.30	0.00	0.00	0.14	0.03	0.00	0.21	0.01	0.00
06BP15*	0.10	0.03	0.00	0.12	0.03	0.00	0.31	0.00	0.00	0.12	0.03	0.00	0.23	0.00	0.00
06BP15*	0.09	0.04	0.01	0.15	0.03	0.00	0.35	0.00	0.00	0.11	0.02	0.00	0.20	0.00	0.00
06BP17*	0.09	0.03	0.00	0.14	0.03	0.00	0.31	0.00	0.00	0.15	0.04	0.00	0.20	0.00	0.00
06BP17*	0.10	0.04	0.01	0.15	0.03	0.00	0.29	0.00	0.00	0.12	0.03	0.00	0.21	0.00	0.00
06BP19	0.11	0.04	0.00	0.14	0.03	0.00	0.28	0.00	0.00	0.13	0.03	0.00	0.22	0.00	0.00
06BP20	0.11	0.03	0.00	0.16	0.03	0.00	0.30	0.00	0.00	0.12	0.03	0.00	0.20	0.00	0.00
06BP21	0.08	0.04	0.01	0.14	0.03	0.00	0.38	0.00	0.00	0.09	0.02	0.00	0.19	0.00	0.00
06BP22*	0.12	0.04	0.00	0.17	0.03	0.00	0.29	0.00	0.00	0.12	0.03	0.00	0.19	0.00	0.00
06BP22*	0.11	0.04	0.00	0.16	0.03	0.00	0.31	0.00	0.00	0.12	0.03	0.00	0.19	0.00	0.00
06BP23*	0.15	0.04	0.01	0.21	0.03	0.00	0.37	0.00	0.00	0.14	0.03	0.00	0.00	0.00	0.00
06BP23*	0.12	0.04	0.00	0.17	0.03	0.00	0.30	0.00	0.00	0.12	0.03	0.00	0.18	0.00	0.00
BP-F-78*	0.09	0.04	0.00	0.13	0.03	0.00	0.26	0.00	0.00	0.14	0.04	0.00	0.24	0.01	0.00
BP-F-78*	0.10	0.05	0.00	0.15	0.04	0.00	0.22	0.00	0.00	0.17	0.04	0.00	0.20	0.01	0.00

06BP24*	0.12	0.04	0.00	0.17	0.03	0.00	0.30	0.00	0.00	0.12	0.03	0.00	0.18	0.00	0.00
06BP24*	0.13	0.03	0.00	0.16	0.02	0.00	0.28	0.00	0.00	0.13	0.03	0.00	0.20	0.00	0.00
BP-A-16	0.13	0.05	0.01	0.14	0.03	0.00	0.23	0.00	0.00	0.15	0.04	0.00	0.20	0.01	0.00
06BP25*	0.12	0.03	0.00	0.16	0.02	0.00	0.28	0.00	0.00	0.13	0.03	0.00	0.21	0.00	0.00
06BP25*	0.12	0.03	0.00	0.16	0.02	0.00	0.29	0.00	0.00	0.13	0.03	0.00	0.20	0.00	0.00
BP-A-17	0.14	0.04	0.01	0.16	0.03	0.00	0.26	0.00	0.00	0.14	0.03	0.00	0.18	0.00	0.00
06BP26*	0.10	0.03	0.00	0.15	0.03	0.00	0.34	0.00	0.00	0.11	0.02	0.00	0.20	0.00	0.00
06BP26*	0.12	0.03	0.00	0.16	0.02	0.00	0.30	0.00	0.00	0.12	0.03	0.00	0.20	0.00	0.00
06BP27*	0.08	0.03	0.00	0.12	0.02	0.00	0.33	0.00	0.00	0.11	0.03	0.00	0.25	0.00	0.00
06BP27*	0.08	0.03	0.00	0.12	0.02	0.00	0.33	0.00	0.00	0.12	0.03	0.00	0.26	0.00	0.00
BP-A-18 1	0.15	0.04	0.00	0.18	0.03	0.00	0.24	0.00	0.00	0.14	0.03	0.00	0.17	0.00	0.00
06BP28*	0.06	0.02	0.00	0.08	0.02	0.01	0.33	0.00	0.00	0.10	0.03	0.01	0.32	0.01	0.00
06BP28*	0.08	0.03	0.00	0.09	0.02	0.00	0.29	0.01	0.00	0.13	0.04	0.00	0.31	0.00	0.00
06BP28*	0.08	0.03	0.00	0.10	0.03	0.00	0.30	0.01	0.00	0.13	0.04	0.00	0.28	0.00	0.00
BP-A-20*	0.07	0.03	0.00	0.10	0.03	0.00	0.31	0.01	0.00	0.11	0.05	0.00	0.28	0.01	0.00
BP-A-20*	0.08	0.03	0.00	0.11	0.03	0.00	0.29	0.01	0.00	0.12	0.05	0.00	0.26	0.01	0.00
BP-A-69*	0.08	0.04	0.00	0.13	0.03	0.00	0.35	0.00	0.00	0.10	0.02	0.00	0.23	0.00	0.00
BP-A-69*	0.09	0.04	0.00	0.14	0.03	0.00	0.32	0.01	0.00	0.11	0.02	0.00	0.23	0.00	0.00

*indicates polar fraction was re-analyzed

Table S2. Data used to generate Figure 4.

Sample number	Elevation (MASL)	CO_2	CO_2min	CO_2max	MST	MSTmin	MSTmax	Char Count	Charmin	Charmax	Pollen
06BP01	300				15.10	13.07	17.13	44	33.31	54.69	
06BP02	300.05	456.1	484.5	427.8				79	62.44	95.56	
06BP03	300.1	458.4	487.9	429	15.38	13.35	17.41	18	14.40	21.61	
06BP04	300.15	400.5	419.3	381.7				20	13.65	26.35	
06BP05	300.2				15.61	13.58	17.64	27	23.39	30.61	
06BP06	300.25	399.7	418.5	381				50	29.79	70.21	
06BP07	300.3	463.7	496	431.3	15.35	13.32	17.38	26	16.93	35.07	1
06BP08	300.35	465.1	498.2	431.9				39	29.36	48.64	1
06BP09	300.4	455.4	483.5	427.4	14.55	12.52	16.58	21	12.81	29.19	1
06BP10	300.45	454.5	482.1	426.9				34	22.85	45.15	
06BP11	300.5	461.9	493.2	430.6	14.91	12.88	16.94	126	88.73	163.27	
06BP12	300.55							19	14.07	23.93	
06BP13	300.6				15.07	13.04	17.10	40	23.80	56.20	
06BP14	300.65	449.5	475.1	424	15.10	13.07	17.13	26	20.49	31.51	
06BP15	300.7	457.9	487.1	428.7	14.67	12.64	16.70	25	13.98	36.02	
06BP16	300.75				14.95	12.92	16.98	18	15	21	
06BP17	300.8	438.5	460.8	416.3	15.21	13.18	17.24	26	21.27	30.72	
06BP18	300.85	468.4	503.7	433.1	14.88	12.85	16.91	20	13.57	26.43	
06BP19	300.9	442.2	465.4	419	15.98	13.95	18.01	29	20.67	37.33	
06BP20	300.95	435	456.4	413.5	14.70	12.67	16.73	28	17.88	38.12	
06BP21	301	442.9	466.3	419.5	14.14	12.11	16.17	33	23.84	42.17	
06BP22	301.05	470	506.5	433.6	14.88	12.85	16.91	25	21.95	28.06	
06BP23	301.1	268.8	289.1	248.5	14.20	12.17	16.23	24	16.19	31.81	
06BP24	301.15	350.4	369.1	331.6	14.99	12.96	17.02	42	39.35	44.65	1
06BP25	301.2				14.82	12.79	16.85	21	14.44	27.56	1
06BP26	301.25	467.3	502.15	432.55	14.41	12.38	16.44	19	15.49	22.512	1
06BP27	301.3	451	477.1	424.9	14.41	12.38	16.44	397	307.28	486.72	
06BP28	301.35	471.1	508.4	433.9	14.79	12.76	16.82	393	304.74	481.26	1
06BP29	301.4							445	320.14	569.86	1
06BP30	301.45							710	385.49	1034.50	1
06BP34	301.65							275	195.00	355.00	
BP-A-20*	~301.35				15.01	12.98	17.04				

*2010 field season sample

Table S3. $^{26}Al/^{10}Be$ burial ages

PDF max age (yr)	1s error +ve (yr)	1s error -ve (yr)	meanvalue (yr)
3.62E+06	1.50E+06	4.78E+05	3.58E+06
3.94E+06	3.66E+06	4.77E+05	NA
4.07E+06	5.79E+06	3.51E+05	NA
3.95E+06	1.49E+06	4.31E+05	3.95E+06

Table S4. Input for burial modeling

Depth cm	Bulk Density g cm^{-3}	Latitude deg	Longitude deg	Surface elevation m	^{10}Be conc atoms g^{-1}	^{10}Be conc err atoms g^{-1}	^{26}Al conc atoms g^{-1}	^{26}Al conc err atoms g^{-1}	Eros Rate cm ka^{-1}
18050	2.2	78.550	-82.373	333	17665	402	26986	7335	2.25
18097	2.2	78.550	-82.373	333	16163	376	22263	7889	2.25
18155	2.2	78.550	-82.373	333	17853	387	22322	10215	2.25
18222	2.2	78.550	-82.373	333	20505	598	26508	7147	2.25

Notes:

1. We attempted a depth-profile type isochron burial date (Balco and Rovey, 2010), however the differences in the measured concentrations were too small and uncertainties in ^{26}Al were too large to define an isochron curve. Therefore we used the more common method of simple burial dating using the relationship of $^{26}Al/^{10}Be$ vs. $\log^{10}Be$, which requires the assumption that the pre-burial ratio of the sand samples was the production ratio of $^{26}Al/^{10}Be$ (6.75).

2. We computed the $^{26}Al/^{10}Be$ burial ages that best fits the measured concentrations, assuming a simple surface buildup and burial history. The depositional environment in the Pliocene was an alluvial fan and pebble-braided-stream system along a mountainous piedmont. Therefore it is reasonable to assume that there was little opportunity for long-term (Ma) deep burial (>20 m) of stored sediment during transport from the nearby mountains. Thus we assume, like most other applications of the simple burial method, that the initial ratio in the sand grains was 6.75 and that only one significant burial event affected the grains in the past 8 Ma (by that time, both isotopes have effectively reached saturation). We use the Lifton et al. (2014) constraints and approach for scaling the production rates in the catchment (buildup) and in the sampled section (post-depositional). The calculations include post-depositional muon production (cosmic ray influx according to Lifton et al., 2014) and erosion of the surface.

3. While the current depth of the samples is approximately 10 m below gravel and till, muons can still penetrate to produce cosmogenic ^{26}Al and ^{10}Be. In other words, the samples are not completely shielded. However, we estimate that there was more sediment and ice above the samples during the Pliocene and Pleistocene as follows: The surface of the Beaufort Formation is more than 40 m higher in elevation across Strathcona Fiord than at BP. Furthermore the region has been significantly eroded since the Pliocene sediment was deposited, as stream paleoflow indicators reveal that the fiord was filled at the time of BP deposition. The amount of erosion in the fiord is much greater than 400 m. We conservatively estimate that 50 m of post-Pliocene erosion occurred above the fiord on the opposite side, or 90 m of sediment loss on the BP side. This would equate to an erosion rate over 4 Ma of 2.25 cm ka^{-1}. Besides sediment with a bulk density of 2.2 g cm^{-3} for coarse sand and sandy gravel, BP would have been covered by ice for the majority of the Quaternary, given its close proximity to the second largest ice field in Canada, Prince of Wales Ice Field. Plateau ice thicknesses are currently >200 m (Kinnard et al., 2008) (i.e. equivalent to approximately 81.8 m of sandy gravel), whereas the ice field is much thicker in valleys and would have been even thicker during much of the Pleistocene. While the mass depth that shielded the samples at any time remains uncertain, our most reasonable estimate is 90.0 +81.8 or 171.8 m of average gravel cover (mass depth = 37.8 x 103 g cm^2). We added 171.8 m to each of the modern sample depths (8.70, 9.17, 9.74, and 10.42 m). While the uncertainty in the actual mass depth is large, a greater shielding thickness does not change the age significantly once depths are greater than 50 m (much deeper burial would yield a slightly younger mean age of 3.6 Ma, while a shallower depth estimate will significantly increase the age beyond the ca. 8 Ma saturation limit. Therefore, we prefer the revised calculated mean burial age over the minimum ages reported in Rybczynski et al. (2013) which were derived using unreasonably great depths and zero erosion (needed for no muogenic production) and a superseded production rate systematics.

4. The mean age of the four samples is 3.9 +1.5/-0.5 Ma. The final most probable ages are therefore our best estimate of burial duration of the Beaver Pond layer. The burial age and error (1σ and 2σ shown in Figure S3) is determined using a systematic parameter search and chi-squared statistic to create a continuous probability density function. We also calculate a burial mean-value age using the FMINLBFGS optimization algorithm (from Matlab file exchange) for comparison with the probability distribution function most probable burial age approach. Those burial mean-value ages were not available for two of the samples because the tails of their pdfs reach beyond the saturation value.

Supplemental References

Balco, G. and Rovey, C. W.: Absolute chronology for major Pleistocene advances of the Laurentide Ice Sheet, Geology, 38, 795–798, 2010.

Kinnard, C., Koerner, R. M., Zdanowicz, C. M., Fisher, D. A., Zheng, J., Sharp, M. J., Nicholson, L., and Lauriol, B.: Stratigraphic analysis of an ice core from the Prince of Wales Icefield, Ellesmere Island, Arctic Canada, using digital image analysis: High-resolution density, past summer warmth reconstruction, and melt effect on ice core solid conductivity, Journal of Geophysical Research: Atmospheres, 113, 2008.

Lifton, N., Sato, T., and Dunai, T. J.: Scaling in situ cosmogenic nuclide production rates using analytical approximations to atmospheric cosmic-ray fluxes, Earth and Planetary Science Letters, 386, 149–160, 2014.

Rybczynski, N., Gosse, J. C., Richard Harington, C., Wogelius, R. A., Hidy, A. J., and Buckley, M.: Mid-Pliocene warm-period deposits in the High Arctic yield insight into camel evolution, Nature Communications, 4, 1–9, 2013.